

PHOTOMECHANICAL STRESS ANALYSIS OF COMPOSITE STRUCTURES

Fatima, N.¹, Ro, Y.¹ Alshaya, A.², Hunt, J.³, ¹and Rowlands, R^{1*}

¹Mechanical Engineering Department, University of Wisconsin-Madison, Madison, WI, USA

² Mechanical Engineering Department, Kuwait University, Kuwait

³ USDA Forest Products Laboratory, Madison, WI, USA

* Corresponding author (rowlands@me.engr.wisc.edu)

Keywords: *Stress Analysis; Digital Image Correlation (DIC); Green and Aerospace Composites*

ABSTRACT

This paper describes ability to stress analyze perforated composite members by processing measured thermal or displacement information with an Airy stress function in real or complex variables. Displacements are measured using digital image correlation whereas an infrared camera records the thermal information. With temperature-related information, the hybrid-method converts the recorded thermal data into individual stress components. If processing displacement data, the method determines the stresses from a single displacement component without physically differentiating measured data. Equilibrium and compatibility conditions are satisfied using real or complex variable formulations and analytic continuation. Processing the measured data with a stress function simultaneously smooths the recorded information and evaluates the individual stress components, including on the edge of a hole or notch. Finite Element and force equilibrium demonstrate reliability of experimental results.

1 INTRODUCTION

Structures made of composite materials frequently contain holes or notches which produce stress concentrations. While stress concentrations themselves might not cause failure, interactions between edge stresses and local material strengths can control structural integrity [1,2]. One may also not know a priori where the most serious stresses occurs on the edge of a cutout. Pure analytical or theoretical stress analyses are typically only available for simple situations having infinite geometries, whereas most practical problems involve complicated, finite shapes. Like numerical (FEM, FDM) approaches, analytical/theoretical analyses depend on knowing the external loading. The latter is often unknown in practice. Moreover, edge data measured by traditional experimental techniques are not reliable, resulting in unreliable edge stresses. Motivated by the above, the ability to stress analyze perforated composite members by processing measured temperature or displacement information using an Airy stress function is described. Both real and complex variable forms of the stress function are utilized.

Displacements are recorded using digital image correlation (DIC). The hybrid-DIC technique reliably provides the three independent stresses from a single measured displacement field. Needing only a single displacement field is advantageous as situations occur where there is a paucity or inferior quality of one or other of the in-plane displacements.

Although classical thermoelastic stress analysis (TSA) provides information on only a linear combination of the stresses, engineering applications such as fatigue or failure theories require knowing the magnitudes of the individual components of stress so it is necessary to “separate the stresses”. The latter can be determined by combining the stress-induced thermal data with some supplementary experimental methods or measured information. Although one could combine TSA with some other experimental method (such as photoelasticity, moiré, speckle) to separate the stresses, it is preferable to use only a single experimental process. The need for other experimental methods or information is circumvented here in that the individual stresses are evaluated by hybridizing the recorded thermal information with analytical and/or numerical tools (Airy stress function and some known boundary conditions).

The described hybrid techniques simultaneously smooth the measured data, satisfy equilibrium and compatibility, and determine individual stresses full-field, including on the edge of holes or notches. This is accomplished without knowing the external loading or physically differentiating the measured information. The latter has its own perils. Applications include those to structural aerospace-type and green (manure-cellulosic) composites.

2 EXPERIMENTAL TECHNIQUES

2.1 *Thermoelastic Stress Analysis (TSA)*

By cyclically loading a structure, the stresses at a location are related to the associated stress-induced temperature changes. Under orthotropy, the recorded signal, S^* , is proportional to the change in the linear combination of the normal stresses, σ_1 and σ_2 , in the directions of material symmetry, *i.e.*,

$$S^* = \Delta(K_1\sigma_1 + K_2\sigma_2) \quad (1)$$

K_1 and K_2 , are traditionally determined experimentally. Recorded TSA data, S^* , at, and adjacent to, an edge are typically unreliable and raw thermoelastic information in composites is inherently noisy. The present technique overcomes these challenges by avoiding the use of recorded data on and near edges and processing the measured interior information with an Airy stress function. The resulting TSA-determined stresses are available on and in the neighborhood of the edge of a hole or notch without knowing the distant geometry or boundary conditions.

2.2 *Digital Image Correlation*

Digital Image Correlation (DIC) is a full-field computer-based image analysis technique for the non-contact measurement of displacements of a surface equipped with a speckle pattern. The method tracks the motion of the speckles by comparing the gray scale value at a point (subset) in a deformed and undeformed configuration. Two sets of images are recorded; the first image typically being at zero load and the second image under load. The achievable DIC resolution depends on a number of factors, including but not limited to, camera resolution, lens optical quality, and speckle size and quality. Unlike electronic speckle, DIC necessitates the surface under study to have a random speckle pattern for tracking; but unlike thermoelastic stress analysis, DIC does not require cyclic loading.

Vic-Snap commercial software (by Correlated Solutions, Inc., Columbia, SC, USA, [3]) was used here to record the images of the plate in its loaded and unloaded conditions and to evaluate the displacements for post-processing. Rather than using the commercial software to provided strains, the DIC-recorded displacement data were processed using the Airy stress function. Quality displacement information at and near the edge of a discontinuity is unavailable because the correlation algorithm is unable to track a group of pixels (subset) which lack neighboring pixels.

3 RELEVANT EQUATIONS

The method behind determining the state of stress at and near the geometrical discontinuity lies in coupling the Airy stress function, with the measured data and imposing traction-free conditions either analytically or discretely, and hence the term *hybrid*.

3.1 Real Variable Formulation

For elasto-static plane problems (plane-stress or plane-strain) in isotropic material with the absence of the body forces, the Airy stress function, Φ , which satisfies stress equilibrium and strains compatibility, gives the biharmonic equation $\nabla^4\Phi = 0$ where ∇^2 is the Laplacian operator and $\nabla^2 = \frac{\partial}{\partial r^2} + \frac{1}{r}\frac{\partial}{\partial r} + \frac{1}{r^2}\frac{\partial}{\partial \theta^2}$. The general solution to $\nabla^4\Phi = 0$ in polar coordinates is [4]

$$\begin{aligned} \Phi = & a_0 + b_0 \ln r + c_0 r^2 + d_0 r^2 \ln r + (A_0 + B_0 \ln r + C_0 r^2 + D_0 r^2 \ln r)\theta \\ & + \left(a_1 r + b_1 r \ln r + \frac{c_1}{r} + d_1 r^3 \right) \sin \theta + \left(a'_1 r + b'_1 r \ln r + \frac{c'_1}{r} + d'_1 r^3 \right) \cos \theta \\ & + (A_1 r + B_1 r \ln r)\theta \sin \theta + (A'_1 r + B'_1 r \ln r)\theta \cos \theta \\ & + \sum_{n=2,3,\dots}^{\infty} (a_n r^n + b_n r^{n+2} + c_n r^{-n} + d_n r^{-(n-2)}) \sin n\theta \\ & + \sum_{n=2,3,\dots}^{\infty} (a'_n r^n + b'_n r^{n+2} + c'_n r^{-n} + d'_n r^{-(n-2)}) \cos n\theta \end{aligned} \quad (2)$$

The individual components of stresses in polar coordinate can be evaluated as

$$\sigma_{rr} = \frac{1}{r} \frac{\partial \Phi}{\partial r} + \frac{1}{r^2} \frac{\partial^2 \Phi}{\partial \theta^2}, \quad \sigma_{\theta\theta} = \frac{\partial^2 \Phi}{\partial r^2}, \quad \sigma_{r\theta} = -\frac{\partial}{\partial r} \left(\frac{1}{r} \frac{\partial \Phi}{\partial \theta} \right) \quad (3)$$

The radial and circumferential displacements are available using Hooke's law and integration from individual components of stresses. The complete form for stresses and displacements are given in reference [1].

Determination of individual stresses, strains, or displacements necessitates evaluating the unknown coefficients in Airy stress function (typically referred to as Airy coefficients). The specific form of the Airy stress function for a particular case can depend on conditions of symmetry, whether or not the coordinate origin is within the component, whether the component is finite or infinite in size (boundedness at origin or infinity), self-equilibrated at individual boundaries, and single-valued stresses, strains and displacements [1].

3.2 Complex Variable Formulation

For plane problems having rectilinear orthotropy and no body forces, the Airy stress function, \mathcal{F} , can be expressed as a summation of two arbitrary analytical functions, $F_1(z_1)$ and $F_2(z_2)$, of the complex variables, z_1 and z_2 , as [5–11]

$$\mathcal{F} = 2\text{Re}[F_1(z_1) + F_2(z_2)] \quad (4)$$

such that $z_j = x + \mu_j y$ for $j = 1, 2$ and Re denotes the 'real part' of a complex number. The complex material properties μ_1 and μ_2 are two distinct roots of the compatibility equation and depend on the constitutive properties ($E_{11}, E_{22}, G_{12}, \nu_{12}$). The stresses in rectangular coordinates (x, y) of the physical $z (= x + iy)$ plane can be expressed in terms of the stress functions. By introducing the new stress functions

$$\Phi(z_1) = \frac{dF_1(z_1)}{dz_1} \quad \text{and} \quad \Psi(z_2) = \frac{dF_2(z_2)}{dz_2} \quad (5)$$

So one can write the stresses as

$$\begin{aligned}\sigma_{xx} &= 2\text{Re}[\mu_1^2\Phi'(z_1) + \mu_2^2\Psi'(z_2)], & \sigma_{yy} &= 2\text{Re}[\Phi'(z_1) + \Psi'(z_2)], & \sigma_{xy} \\ &= -2\text{Re}[\mu_1\Phi'(z_1) + \mu_2\Psi'(z_2)]\end{aligned}\quad (6)$$

where primes denote differentiation with respect to the argument. The stresses satisfy equilibrium and associated strains satisfy compatibility. The displacements can be written in terms of the stress functions as

$$u = 2\text{Re}[p_1\Phi(z_1) + p_2\Psi(z_2)] - w_0y + u_0, \quad v = 2\text{Re}[q_1\Phi(z_1) + q_2\Psi(z_2)] + w_0y + v_0 \quad (7)$$

where w_0 , u_0 , and v_0 are constants of integration and characterize any rigid body translations (u_0 and v_0) and rotation (w_0). The other quantities, which depend on material properties, are

$$p_1 = \frac{\mu_1^2}{E_{11}} - \frac{\nu_{12}}{E_{11}}, \quad p_2 = \frac{\mu_2^2}{E_{11}} - \frac{\nu_{12}}{E_{11}}, \quad q_1 = -\frac{\nu_{12}}{E_{11}}\mu_1 + \frac{1}{E_{22}\mu_1}, \quad q_2 = -\frac{\nu_{12}}{E_{11}}\mu_2 + \frac{1}{E_{22}\mu_2} \quad (8)$$

When the plate is loaded physically in a testing machine, the rigid body motions, u_0 , v_0 , and w_0 are zero. Plane problems of elasticity classically involve determining the stress functions, $\Phi(z_1)$ and $\Psi(z_2)$, throughout a component and subject to the boundary conditions around its entire edge. For a region of a component adjacent to a traction free-edge, $\Phi(z_1)$ and $\Psi(z_2)$ can be related to each other by the conformal mapping and analytic continuation techniques. One can express the stresses in terms of the single stress function, $\Phi(z_1)$. Moreover, $\Phi(z_1)$ will be represented by a truncated power-series expansion whose unknown complex coefficients are determined experimentally. Once $\Phi(z_1)$ and $\Psi(z_2)$ are evaluated, the individual stresses and displacements are known from equations (6). For a significantly large region of interest in a finite structure, it may also be necessary to satisfy other boundary conditions at discrete locations.

3.2.1 Conformal Mapping

Conformal mapping is introduced to simplify the plane problem by mapping the region R_z of a complicated physical $z = x + iy$ plane of a loaded physical component into a region R_ζ of a simpler shape in the $\zeta = \xi + i\eta$ plane. The boundary Γ of the physical z -plane is mapped into the inner boundary Γ_ζ of the unit circle if one represents the stress function as a Laurent series, Figure 1 [1,5–8].

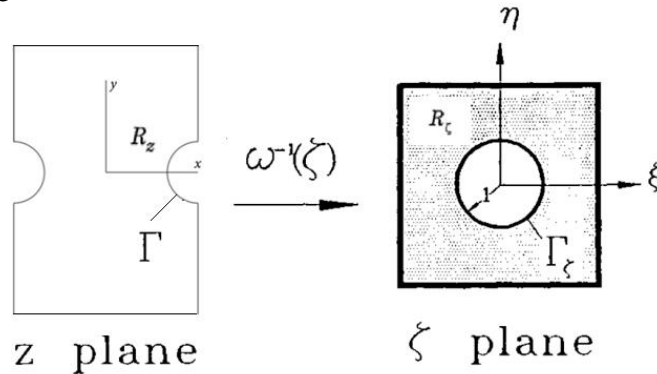


Figure 1: Mapping a circular cutout in the physical z -plane into exterior region of a unit circle in ζ -plane.

Assume that a mapping function of the form $z = \omega(\zeta)$ exists and which maps R_ζ of the simpler plane into R_z of the more complicated physical plane. For orthotropy, the following auxiliary planes and their induced mapping functions are defined in terms of $\zeta_j = \xi + \mu_j\eta$

$$z_j = \omega_j(\zeta_j), \quad j = 1, 2 \quad (9)$$

The induced conformal mapping functions are one-to-one and invertible. The stress functions $\Phi(z_1)$ and $\Psi(z_2)$ can be expressed as the following analytic functions of ζ_1 and ζ_2 .

$$\Phi(z_1) = \Phi[\omega_1(\zeta_1)] \equiv \Phi(\zeta_1), \quad \Psi(z_2) = \Psi[\omega_2(\zeta_2)] \equiv \Psi(\zeta_2) \quad (10)$$

Derivatives of the stress functions with respect to their argument are

$$\Phi'(z_1) = \Phi'(\zeta_1) \frac{d\zeta_1}{dz_1} = \frac{\Phi'(\zeta_1)}{\omega_1'(\zeta_1)}, \quad \Psi'(z_2) = \frac{\Psi'(\zeta_2)}{\omega_2'(\zeta_2)} \quad (11)$$

The analyticity of the mapping functions satisfies the equilibrium and compatibility throughout region R_z of the physical plane.

3.2.2 Traction-free boundaries

Using the concept of analytic continuation, the individual stress functions for a region R_ζ adjacent to a traction-free boundary of the unit circle of an orthotropic material are related by [9,10]

$$\Psi(\zeta_2) = B\Phi(1/\bar{\zeta}_2) + C\Phi(\zeta_2) \quad (12)$$

where B and C are

$$B = \frac{\bar{\mu}_2 - \bar{\mu}_1}{\mu_2 - \bar{\mu}_2}, \quad C = \frac{\bar{\mu}_2 - \mu_1}{\mu_2 - \bar{\mu}_2} \quad (13)$$

Equation (12) enable the elastic strains and stresses of the structure to be expressed in terms of a single stress function, $\Phi(\zeta_1)$, the latter which can be represented by a Laurent series expansion.

3.2.3 Mapping Formulation

For a region adjacent the circular notch of radius R , the following function [11]

$$z_j = \omega_j(\zeta_j) = \frac{R}{2} \left[(1 - i\mu_j)\zeta_j + \frac{1 + i\mu_j}{\zeta_j} \right], \quad j = 1, 2 \quad (14)$$

maps the region of the exterior of a unit circle, R_ζ , of the ζ -plane into the region R_z of the z -physical plane, Figure 2. The inverse of the induced mapping function is

$$\zeta_j = \omega_j^{-1}(z_j) = \frac{z_j \pm \sqrt{z_j^2 - R^2(1 + \mu_j^2)}}{R(1 - i\mu_j)}, \quad j = 1, 2 \quad (15)$$

The branch of the square root in equation (15) is chosen such that $|\zeta_j| \geq 1$ for $j = 1, 2$. The mapping function for elliptical cutout is given in reference [12].

3.2.4 Mapping Collocation, Stresses and Displacements

The single stress function can be expresses as the following finite Laurent series [1]

$$\Phi(\zeta_1) = \sum_{\substack{j=-N \\ j \neq 0}}^N A_j \zeta_1^j \quad (16)$$

where $A_j = a_j + ib_j$ are the unknown complex coefficients (a_j and b_j are both real numbers). The $j = 0$ term contributes to rigid-body motion and can be omitted. The stress function can also be represented by Taylor series [1]. Substituting equation (16) into (12) yields

$$\Psi(\zeta_2) = \sum_{\substack{j=-N \\ j \neq 0}}^N (\bar{A}_j B \zeta_2^{-j} + A_j C \zeta_2^j) \quad (17)$$

where \bar{A}_j is the complex conjugate of A_j . At least for a finite, simply connected region R_ζ , $\Phi(\zeta_1)$ is a single-valued analytic function. Orthotropic composite whose complex parameters are purely imaginary when the directions of material symmetry are parallel and perpendicular to the applied load require retaining only odd terms in the Laurent expansions. Upon combining equations (6), (11), (16), and (17) the individual stresses become

$$\sigma_{xx} = 2 \sum_{\substack{j=-N, \dots \\ j \neq 0}}^N \operatorname{Re} \left\{ j \left[\frac{\mu_1^2 \zeta_1^{j-1}}{\omega_1'(\zeta_1)} + \frac{C \mu_2^2 \zeta_2^{j-1}}{\omega_2'(\zeta_2)} \right] A_j - j \mu_2^2 B \left[\frac{\zeta_2^{-j-1}}{\omega_2'(\zeta_2)} \right] \bar{A}_j \right\} \quad (18)$$

$$\sigma_{yy} = 2 \sum_{\substack{j=-N, \dots \\ j \neq 0}}^N \operatorname{Re} \left\{ j \left[\frac{\zeta_1^{j-1}}{\omega_1'(\zeta_1)} + \frac{C \zeta_2^{j-1}}{\omega_2'(\zeta_2)} \right] A_j - j B \left[\frac{\zeta_2^{-j-1}}{\omega_2'(\zeta_2)} \right] \bar{A}_j \right\} \quad (19)$$

$$\sigma_{xy} = -2 \sum_{\substack{j=-N, \dots \\ j \neq 0}}^N \operatorname{Re} \left\{ j \left[\frac{\mu_1 \zeta_1^{j-1}}{\omega_1'(\zeta_1)} + \frac{C \mu_2 \zeta_2^{j-1}}{\omega_2'(\zeta_2)} \right] A_j - j \mu_2 B \left[\frac{\zeta_2^{-j-1}}{\omega_2'(\zeta_2)} \right] \bar{A}_j \right\} \quad (20)$$

From equations (7), the displacements can be written as

$$u = 2 \sum_{\substack{j=-N, \dots \\ j \neq 0}}^N \operatorname{Re} \{ [p_1 \zeta_1^j + p_2 C \zeta_2^j] A_j + p_2 B \zeta_2^{-j} \bar{A}_j \} \quad (21)$$

$$v = 2 \sum_{\substack{j=-N, \dots \\ j \neq 0}}^N \operatorname{Re} \{ [q_1 \zeta_1^j + q_2 C \zeta_2^j] A_j + q_2 B \zeta_2^{-j} \bar{A}_j \} \quad (22)$$

Choosing the y -axis parallel to the strongest, stiff orientation of the composite, Fig. 1, *i.e.*, 1-direction of an orthotropic composite material, and introducing the Laurent series according to equation (1), the thermoelastic data S^* becomes

$$\begin{aligned} S^* &= K_1 \sigma_{yy} + K_2 \sigma_{xx} \\ &= 2 \sum_{\substack{j=-N, \dots \\ j \neq 0}}^N \operatorname{Re} \left\{ \left[\frac{j(K_1 + K_2 \mu_1^2)}{\omega_1'(\zeta_1)} \zeta_1^{j-1} + \frac{j(K_1 + K_2 \mu_2^2) C}{\omega_2'(\zeta_2)} \zeta_2^{j-1} \right] A_j \right. \\ &\quad \left. - \left[\frac{j(K_1 + K_2 \mu_2^2) B}{\omega_2'(\zeta_2)} \zeta_2^{-j-1} \right] \bar{A}_j \right\} \end{aligned} \quad (23)$$

The only unknowns in these expressions for the stresses and displacements are the complex coefficients $A_j = a_j + ib_j$, the other quantities involve geometry (location) or material properties. These coefficients can be determined from measured displacement or temperature data. Using conformal mapping and analytic continuation techniques, equations (18) through (20) imply that the stresses satisfy equilibrium and traction-free conditions along the adjacent portion of the entire boundary. However, unlike a classical boundary-value problem where one would typically evaluate the unknown coefficients, A_j , by satisfying the boundary and loading conditions around the entire shape, one can use a combination of the measured stresses of equations (18) through (20) and/or displacements of equations (21) and (22) from within region R_z to determine these unknown complex coefficients, A_j . One can also impose additional known boundary conditions at discrete locations. The concept of collecting measured data in a region R^* adjacent to an edge Γ , mapping R_z into R_ζ such that Γ of the physical z -plane is mapped into the unit circle in the ζ -plane

whereby the traction-free conditions on Γ are satisfied continuously, relating the two complex stress functions to each other, plus satisfying other loading conditions discretely on the boundary of the component beyond Γ will be referred to as the mapping-collocation technique.

The non-boundary values of displacement u^* or v^* or temperature information S^* at m different locations within region R^* and q known stress conditions at discrete points are employed. A system of simultaneous linear equations $[A]_{(m+q) \times 4N} \{c\}_{4N \times 1} = \{A^*\}_{(m+q) \times 1}$, is formed whose matrix $[A]$ consists of analytical expressions for u^* or v^* or S^* and the those of the known stress conditions, vector $\{c\} = \{a_{-N}, b_{-N}, a_{-N+1}, b_{-N+1}, \dots, a_{N-1}, b_{N-1}, a_N, b_N\}$ has $4N$ unknown real coefficients, and vector $\{A^*\}$ includes the m measured displacement values or TSA signal S^* and q discretely imposed stress conditions such that $m + q \gg 4N$. The best values of the coefficients A_j can then be determined in a least-squares numerical sense. The variables $\zeta_j = \xi + \mu_j \eta$, in equations (18) through (22) are related to the physical locations $z = x + iy$ through the inverse mapping function $z_j = \omega_j(\zeta_j)$ of equation (14) through (15). The individual stresses then are known throughout the region, R_z , including on the traction-free edge Γ from equations (18) through (20). The number of terms, N , to retain in the stress function is typically selected by evaluating the difference between the magnitude of experimentally based data and those predicted according to the present hybrid method by using root mean square approach.

4 EXAMPLES

Recognizing the general inability to analyze orthotropic materials using real variables, several stress analyses of orthotropic composites have utilized an Airy stress function in complex variables and conformal mapping. Lin and Rowlands [13] analyzed a notched orthotropic laminated plate thermoelastically, Hawong et. al. [14] combined measured isochromatic information and a complex stress function to study the stresses in a circularly-perforated composite whereas Rhee and Rowlands [15] thermoelastically determined the edge stresses of a circular hole and the stress intensity factors in a composite having a crack. Baek and Rowlands used conformal mapping with moiré [16] and strain gage data [17] to determine the full-field stress around a circular hole in composite plate. Ju and Rowlands [18,19] determined stress intensity factors thermoelastically for inclined cracks in an orthotropic composite. All of these prior applications of the mapping technique either separated stresses from recorded isopachic or isochromatic information or evaluated the stresses using two components of displacement whereas the present displacement-based approaches utilize only one recorded displacement component to evaluates all the stresses.

4.1 Thermoelastic Stress Analysis

The full-field stresses in loaded, perforated cellulosic-manure composites from recorded temperature information was determined using the Airy stress in the real variable, equation (2), and imposing traction-free conditions, $\sigma_{rr} = \sigma_{r\theta} = 0$ on the boundary of the hole, Figure 2 [20]. Being able to stress analyze such green materials addresses several societal issues; include providing engineering members fabricated from materials which are suitable for developed and developing nations, relieving a troubling by-product of agricultural regions and reducing demands on our landfills. Alshaya et al. [21] employed recorded temperature data, S^* , to stress analyzed a finite graphite/epoxy laminated orthotropic composite containing an elliptical hole using mapping collocation technique as shown in Figure 3.

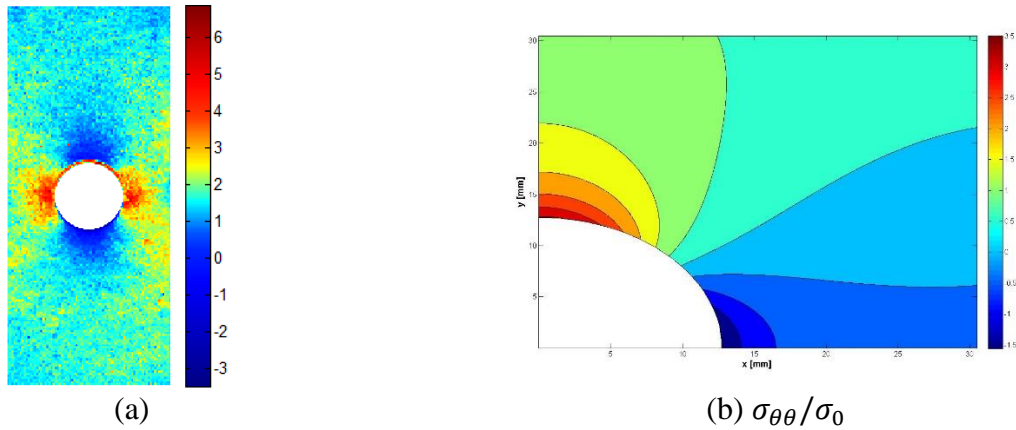


Figure 2: (a) TSA recorded signals in cellulose-manure composite and (b) Contour plot of $\sigma_{\theta\theta}/\sigma_0$ throughout the region adjacent to the circular hole by hybrid-TSA; $m = 10,000$ and 7 Airy coefficients [20].

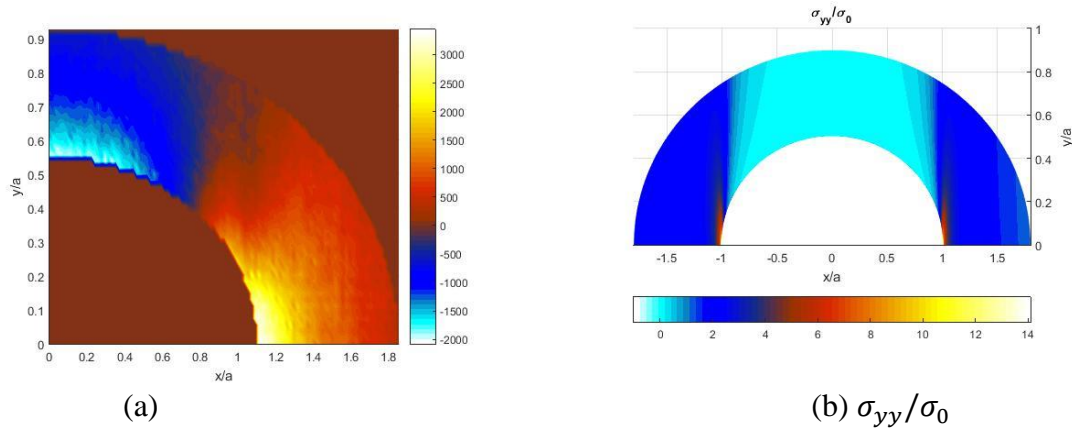


Figure 3: (a) Thermoelastic data, S^* , as averaged throughout the four quadrants (load range = 7.12 kN) in graphite-epoxy composite and (b) Contour plot of σ_{yy}/σ_0 throughout the region adjacent to the elliptical hole by FEA (right) and hybrid-TSA; $m = 2,558$ and 8 real coefficients (right) [21].

4.2 Digital Image Correlation

A finite graphite/epoxy laminated composite plate containing symmetrically-located sided-notches and vertically loaded in the strongest/stiffest material direction is analyzed, Figure 4 [22]. The DIC-recorded displacement data employed are those in the loading direction. Stresses at and in the vicinity of the edge of a side notch are illustrated in Figure 4(b). Reference [23] provides further information regarding employing different amounts and source locations of measured displacements and varying number of coefficients, as well as how displacements are differentiated to provide strains. Figure 5 shows the DIC-determined stresses around a hole in a loaded graphite/epoxy laminate from only measured vertical displacement information [24].

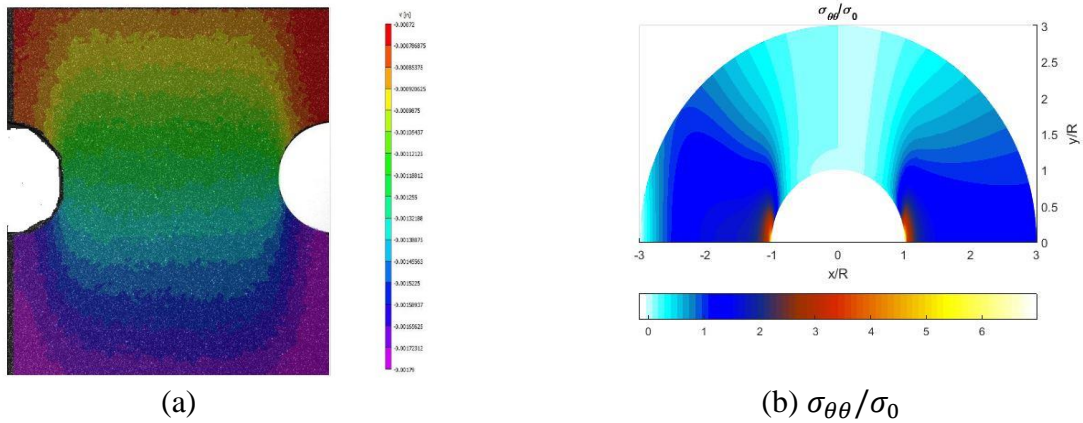


Figure 4: (a) DIC recorded v -displacement in graphite-epoxy composite and (b) Contour plot of $\sigma_{\theta\theta}/\sigma_0$ throughout the region adjacent to the notch by FEA (right) and hybrid-DIC; $m = 2,200$, $q = 24$ and 12 real coefficients (left) [22].

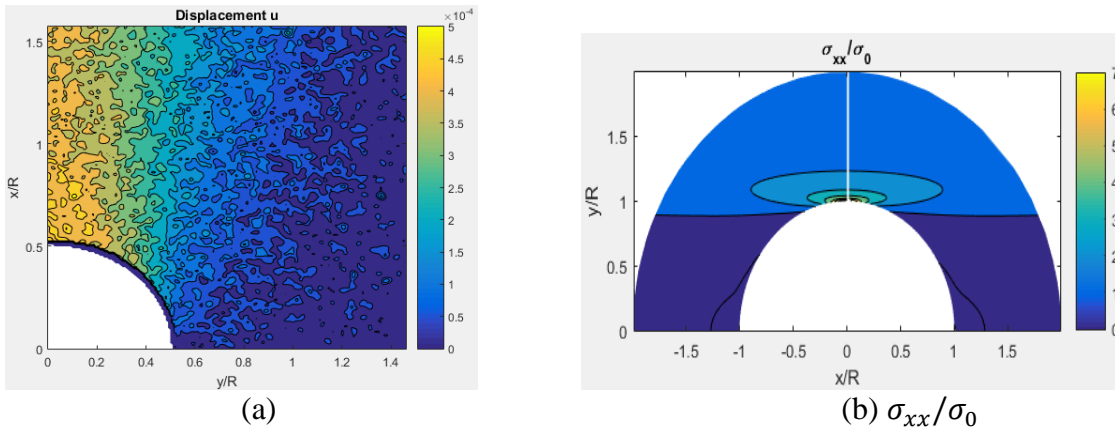


Figure 5: (a) DIC recorded v -displacement data in graphite-epoxy composite and (b) Contour plot of σ_{xx}/σ_0 throughout the region adjacent to the hole by FEA (left) and hybrid-DIC; $m = 6,448$, $q = 10,803$ and 4 real coefficients (right) [23].

5 SUMMARY AND CONCLUSIONS

The successful ability to stress analyze perforated composite members by processing measured thermal or displacement information using an Airy stress function is described.

6 REFERENCES

- [1] Alshaya, A. A., 2017, “Experimental, Analytical and Numerical Analyses of Orthotropic Materials and Biomechanics Application,” PhD Thesis, University of Wisconsin-Madison.
- [2] Rhee, J., Cho, H.-K., Marr, D. J., and Rowlands, R. E., 2012, “Local Compliance, Stress Concentrations and Strength in Orthotropic Materials,” *J. Strain Anal. Eng. Des.*, **47**(2), pp. 113–128.
- [3] Correlated Solutions, “Principle of Digital Image Correlation” [Online]. Available: <http://www.correlatedsolutions.com/index.php/principle-of-digital-image-correlation>.

- [4] Soutas-Little, R. W., 1999, *Elasticity*, Dover Publications, Mineola, NY.
- [5] Lekhnitskii, S. G., 1968, *Anisotropic Plates*, Gordon & Breach Scientific Publishers, New York.
- [6] Lin, S. T., and Rowlands, R. E., 1999, "Hybrid Stress Analysis," *Opt. Lasers Eng.*, **32**(3), pp. 257–298.
- [7] Muskhelishvili, N., 1977, *Some Basic Problems of the Mathematical Theory of Elasticity*, Springer, Leyden.
- [8] Savin, G. N., 1961, *Stress Concentration Around Holes*, Pergamon Press.
- [9] Bowie, O. L., and Freese, C. E., 1972, "Central Crack in Plane Orthotropic Rectangular Sheet," *Int. J. Fract. Mech.*, **8**(1), pp. 49–57.
- [10] Gerhardt, T. D., 1984, "A Hybrid/Finite Element Approach for Stress Analysis of Notched Anisotropic Materials," *J. Appl. Mech.*, **51**(4), pp. 804–810.
- [11] Lekhnitskii, S. G., 1963, *Theory of Elasticity of an Anisotropic Elastic Body*, Holden-Day, San Francisco.
- [12] Alshaya, A., Shuai, X., and Rowlands, R., 2017, "Stress Analysis of a Finite Orthotropic Plate Containing an Elliptical Hole from Recorded Temperature Data," *Residual Stress, Thermomechanics & Infrared Imaging, Hybrid Techniques and Inverse Problems, Volume 9: Proceedings of the 2016 Annual Conference on Experimental and Applied Mechanics*, S. Quinn, and X. Balandraud, eds., Springer International Publishing, Cham, pp. 47–56.
- [13] Lin, S. T., and Rowlands, R. E., 1995, "Thermoelastic Stress Analysis of Orthotropic Composites," *Exp. Mech.*, **35**(3), pp. 257–265.
- [14] Hawong, J. S., Lin, C. H., Lin, S. T., Rhee, J., and Rowlands, R. E., 1995, "A Hybrid Method to Determine Individual Stresses in Orthotropic Composites Using Only Measured Isochromatic Data," *J. Compos. Mater.*, **29**(18), pp. 2366–2387.
- [15] Rhee, J., and Rowlands, R. E., 1999, "Thermoelastic-Numerical Hybrid Analysis of Holes and Cracks in Composites," *Exp. Mech.*, **39**(4), pp. 349–355.
- [16] Baek, T. H., and Rowlands, R. E., 1999, "Experimental Determination of Stress Concentrations in Orthotropic Composites," *J. Strain Anal. Eng. Des.*, **34**(2), pp. 69–81.
- [17] Baek, T., and Rowlands, R., 2001, "Hybrid Stress Analysis of Perforated Composites Using Strain Gages," *Exp. Mech.*, **41**(2), pp. 195–203.
- [18] Ju, S. H., and Rowlands, R. E., 2003, "Mixed-Mode Thermoelastic Fracture Analysis of Orthotropic Composites," *Int. J. Fract.*, **120**(4), pp. 601–621.
- [19] Ju, S. H., and Rowlands, R. E., 2003, "Thermoelastic Determination of KI and KII in an Orthotropic Graphite–epoxy Composite," *J. Compos. Mater.*, **37**(22), pp. 2011–2025.
- [20] Ro, Y. H., Hunt, J., and Rowlands, R., "Stress Analysis of Cellulosic-Manure Composites," *J. Wood Fiber Sci.*, (Submitted).
- [21] Alshaya, A., Shuai, X., and Rowlands, R., 2016, "Thermoelastic Stress Analysis of a Finite Orthotropic Composite Containing an Elliptical Hole," *Exp. Mech.*, **56**(8), pp. 1373–1384.
- [22] Alshaya, A., and Rowlands, R., 2017, "Experimental Stress Analysis of a Notched Finite Composite Tensile Plate," *Compos. Sci. Technol.*, **144**, pp. 89–99.
- [23] Alshaya, A. A., and Rowlands, R., "Experimental Stress Analysis of a Notched Finite Composite Tensile Plate," *Compos. Sci. Technol.*, (In press).
- [24] Fatima, N. S., 2017, "Hybrid Photomechanical Full-Field Stress Analysis of Orthotropic Composite Structures Containing Various Cutouts," PhD Thesis, University of Wisconsin-Madison.